

## Parameter space of low frequency inter-ELM modes

B. Vanovac<sup>1</sup>, E. Wolfrum<sup>2</sup>, M. Willensdorfer<sup>2</sup>, M. Griener<sup>2</sup>,

A. F. Mink<sup>2</sup>, G. F. Harrer<sup>3</sup>, M. Hoelzl<sup>2</sup>, and the ASDEX Upgrade Team

<sup>1</sup> *DIFFER - Dutch Institute for Fundamental Energy Research, Eindhoven, the Netherlands*

<sup>2</sup> *Max-Planck-Institut für Plasmaphysik, 85748 Garching, Germany*

<sup>3</sup> *Institute of Applied Physics, TU Wien, Fusion@ÖAW, 1040 Vienna, Austria*

**Introduction:** The ELM cycle of type-I ELMs consists of different phases characterized by the evolution of kinetic profiles on different time scales [1] and distinct MHD and turbulence activity. In the latest phase of the ELM cycle, the pressure gradients are clamped. During this phase low [2], medium [3] and high frequency [4] MHD modes develop simultaneously in the steep gradient region. The high-frequency modes are located close to the minimum of the  $E_r$  well, and are measured as fluctuations in the radial magnetic field on both, low and high field side [4]. The focus of the work presented here is the low-frequency modes. The low frequency modes are measured only at the low field side and are located further inwards, towards the pedestal top [5]. They appear as fluctuations in the electron density, the electron temperature and as magnetic fluctuations. These modes rotate poloidally in the electron diamagnetic direction with the velocity of the background flow at that position [5]. The nature of this mode is not yet clear. In this work, we show the dependences of the low-frequency mode characteristics on some of the plasma and ELM parameters.

**Results:** An example of a power spectrum, in the low and the high-frequency range for inter-ELM synchronized measurements during the discharge #34347, is shown in figure 1. On the left panel, the mean amplitude of four different Electron Cyclotron Emission (ECE) radial channels is depicted, showing the activity in the low frequency range of the spectrum during the inter-ELM phase. The resonant positions are color-coded and span from the Scrape-Off Layer (SOL) region towards the confined region, close to the pedestal top. Increased power in the spectrum is measured in the range of 10 kHz in all shown channels. The outermost channel, resonant around the separatrix at  $\rho_{\text{pol}} = 1.007$ , measure the emission of the relativistically down-shifted electrons from the pedestal region [6]. The channel closest to the separatrix (in green), resonant inside the confined region, shows two prominent peaks. The first peak, at 10 kHz corresponds to the fundamental frequency of the mode, and the second one to its harmonic. The largest amplitude (shown in red) is measured in the signal resonant at the position of the steepest temperature gradient. The mode is also measured further inside, at  $\rho_{\text{pol}} = 0.978$ . On the right panel, an average spectral amplitude during an inter-ELM phase, measured with the magnetic pick-up coil is

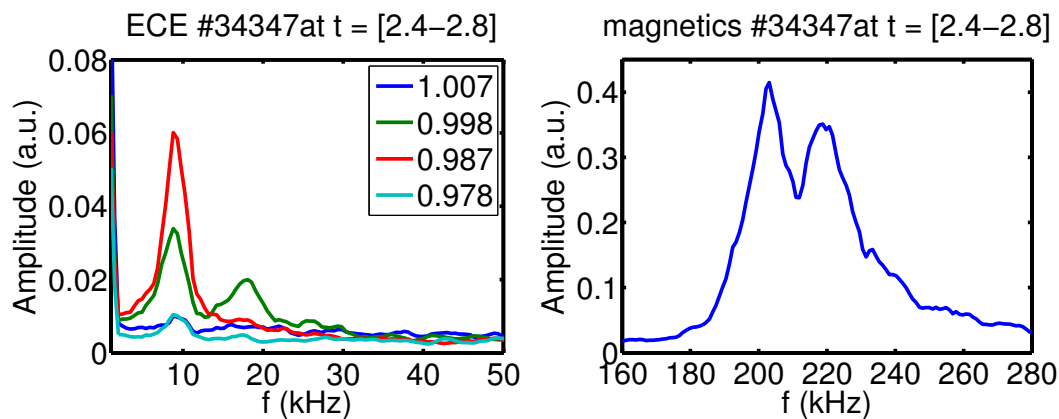


Figure 1: ELM synchronized amplitude spectrum of radially resolved ECE channels (left) for the low- $f$  mode, and magnetic pick-up coil (right) for the high- $f$  mode. Radial channel of the ECE are color-coded. Both diagnostics measure on the low field side.

shown. This coil is located on the low field side, and measures the changes in the radial magnetic field. Multiple peaks in the Fourier spectrum appear, although there are two prominent ones; the one at 206 kHz and the one at 220 kHz. The low-frequency modes differ for individual ELMs, which makes the ELM synchronized analysis quite obscure when it comes to examining the fine structure and temporal resolution during an inter-ELM phase. However, to examine the tendencies, the comparison with specific plasma parameters and discharge conditions is possible with the ELM-synchronization approach. Therefore, we examine seventeen different phases of various discharges, where the low frequency modes are detected in the average amplitude spectrum (see figure 1(left)), and look at the behaviour of the low-frequency mode against plasma and ELM parameters. Parameters were constant during the averaging times. The top panel of figure 2 shows the dependence of the low frequency and high-frequency modes on the input power ( $P$ ). Color-coded is the Electron Cyclotron Resonance Heating (ECRH), Neutral Beam Injection (NBI) and the total power ( $P_{\text{ECRH}} + P_{\text{NBI}}$ ). As shown,  $f_{\text{LOW}}$  decreases with increasing input power (shown in figure 3 (a)). This change in frequency of the low-frequency mode is mainly driven by the increase in the toroidal rotation concomitant with the increase in NBI power which is consistent with previous observations reported in [5]. No explicit dependence on the ECRH power is observed. Contrary to this observation, the high-frequency modes ( $f_{\text{HIGH}}$ ) do not show the dependence on the increase in the toroidal rotation in the range of powers discussed in this work (see figure 3 (b)). Their frequency remains in the range of 220 - 240 kHz. This observation suggests that either the high-frequency modes are not affected by the change in toroidal rotation at all or, as their frequency is mainly driven by the poloidal flow, for such a high frequency the

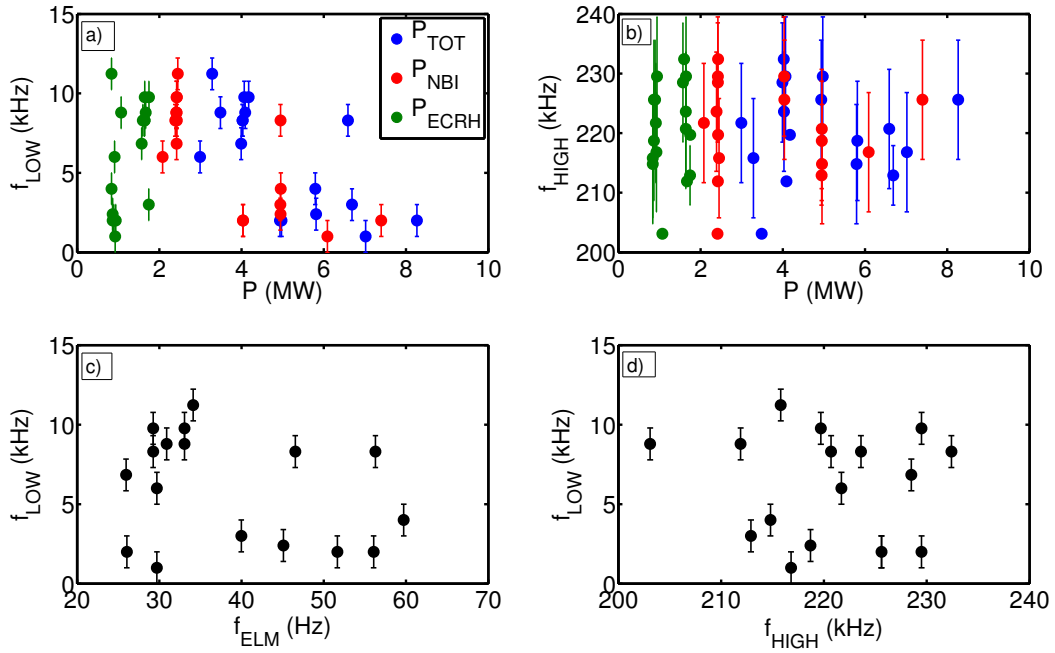


Figure 2: Frequency dependence of the low ( $f_{\text{LOW}}$ ) (a) and high ( $f_{\text{HIGH}}$ ) (b) frequency modes on the input ECRH, NBI and total power. In the bottom panels frequency of the low frequency modes is plotted against ELM repetition frequency ( $f_{\text{ELM}}$ ) (c) and frequency of the high frequency modes ( $f_{\text{H}}$ ) (d).

toroidal component is negligible. In the bottom panel, we show the span of the low-frequency modes with respect to the ELM repetition frequency ( $f_{\text{ELM}}$ ). As presented, the low frequency ELMs are measured only in the phases featuring low ELM repetition rate (30 kHz to 60 kHz). At the same time the high-frequency modes ( $f_{\text{HIGH}}$ ) are measured in a range of 210 kHz to 230 kHz (figure 2 (d)). No correlation of  $f_{\text{LOW}}$  with either  $f_{\text{ELM}}$  or  $f_{\text{HIGH}}$  can be observed. An analysis of the frequency dependence on parameters relevant for drive or stability of MHD modes is shown in figure 3. The frequency of the low-frequency modes decreases for an increase in  $\beta_{\text{pol}}$  (see figure 3(a)). The  $\beta_{\text{pol}}$  is defined as the the volume averaged pressure across the whole plasma, normalized by the average squared poloidal magnetic field. The pedestal pressure dependence shows no clear trend (b). The dependence on the normalized pressure gradient (d) also shown similar dependence as  $\beta_{\text{pol}}$ . As the  $q_{95}$  parameter space (c) does not vary significantly, this dependence is mainly due to the pressure gradient term. This term is a crucial drive for variety of MHD instabilities.

So far, the main feature found in this work relates to the change in frequency of the low frequency modes for an extended range of input powers. This dependence will be compared

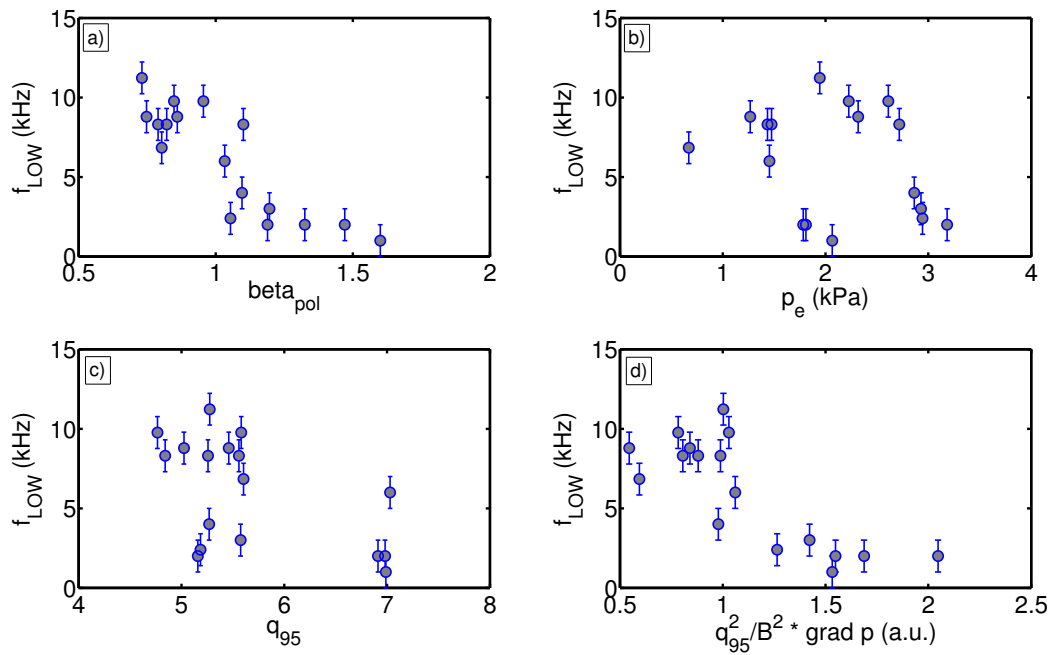


Figure 3: Frequency dependence of the low ( $f_{\text{LOW}}$ ) frequency mode on: (a) normalized poloidal pressure ( $\beta_{\text{pol}}$ ), (b) pedestal pressure ( $p_e$ ) evaluated at  $\rho_{\text{pol}}$  of 0.98, (c) edge safety factor ( $q_{95}$ ) and (d) normalized pressure gradient.

with direct measurements of the toroidal rotation. Further improvements involve an increase of the range of parameters, an extension towards scenarios where the modes are not observed which might help target the thresholds for appearance of the low frequency mode, and possibly help gain more insight into its origin.

### Acknowledgements

G. F. Harrer is a fellow of the Austrian Friedrich Schiedel Foundation for Energy Technology. This work has been carried out within the framework of the EUROfusion Consortium and has received funding from the Euratom research and training programme 2014-2018 under grant agreement No 633053. The views and opinions expressed herein do not necessarily reflect those of the European Commission.

### References

- [1] A Burckhart et al, Plasma Physics and Controlled Fusion (2010)
- [2] B Vanovac et al, Plasma Physics and Control Fusion (2018)
- [3] F A Mink et al, Plasma Physics and Control Fusion (2016)
- [4] F M Laggner et al, Plasma Physics Control Fusion (2016)
- [5] B Vanovac et al, submitted to Nuclear Fusion
- [6] S S Denk et al, EPJ Web Conferences (2017)